

## Wire fractures in locked coil cables

K. GJERDING-SMITH†, R. JOHNSEN‡, H. I. LANGE§, B. H. LEINUM¶, G. GUNDERSEN||,  
B. ISAKSEN\*|| and G. NÆRUM||

†Consulting Engineers Haug og Blom-Bakke AS, Oslo, Norway

‡The Norwegian University of Science and Technology (NTNU), Trondheim, Norway

§SINTEF, Trondheim, Norway

¶Det Norske Veritas, Oslo, Norway

||Norwegian Public Roads Administration, Oslo, Norway

(Revised version received 2 June 2006)

Wire fractures in the main cables of the Lysefjord Suspension Bridge display an approximate linear relationship with time. Uncertainties related to wire fractures in sub-layers, reduction of load-carrying capacity and lifetime, and future development of wire fractures have prompted extensive investigations of the main cables. Failure analyses of fractured Z-wire samples and fracture mechanics analysis concluded that cracks have initiated and propagated from surface imperfections. The potential for hydrogen atom generation and absorption that causes hydrogen-induced cracking is discussed. Hydrogen atoms result from the hot-dip galvanization process, or due to corrosion. Evaluation of remaining load-carrying capacity and the need for strengthening of the main cables are briefly discussed and methods for surveillance of wire fractures are presented.

**Keywords:** Suspension bridge; Cable wire; Failure analysis; Fracture mechanics; Corrosion; High-strength steel

### 1. Introduction

The Norwegian Public Roads Administration (NPR) has more than 80 years of experience with suspension bridges and locked coil cables, and today NPR operate and maintain more than 60 suspension bridges. The Lysefjord Suspension Bridge is located on the western coast of Norway, roughly 25 km east of the city of Stavanger, and crosses Lysefjord with a main span of 446 m. Since its completion in 1997 more than 900 wire fractures have been identified in the outer layer of the main cables.

#### 1.1 Bridge and cable geometry

A schematic overview of the Lysefjord Bridge is given in figure 1. Figure 2 shows a cross-section of the main cables on each side, where six prefabricated full-locked coil cables with nominal diameter of 97 mm are arranged in one layer.

The cross-section of the cable is shown in figure 2, i.e. the core wire, four (five) layers of round wire, and five layers of Z-wire. One layer is fill-wire indicated as (6)<sub>1.95</sub> in the expression below. The total of 279 individual wires are assembled as follows:

$$1_{4.95} + 6_{4.75} + (6)_{1.95} + 12_{4.4} + 18_{4.4} + 24_{4.4} \\ + 33Z_{5.0} + 37Z_{5.5} + 41Z_{6.0} + 47Z_{6.0} + 54Z_{6.0}$$

where the indices represent diameter of round wires or height of Z-wires. The parenthesis in the third term indicates fill-wires.

#### 1.2 Fracture registrations

No indications of wire fractures in the main cables were discovered when the bridge was completed in 1997. In July 1999, a visual cable inspection discovered 56 wire fractures. Since then, visual inspections of new fractures are

\*Corresponding author. Email: bjorn.isaksen@vegvesen.no

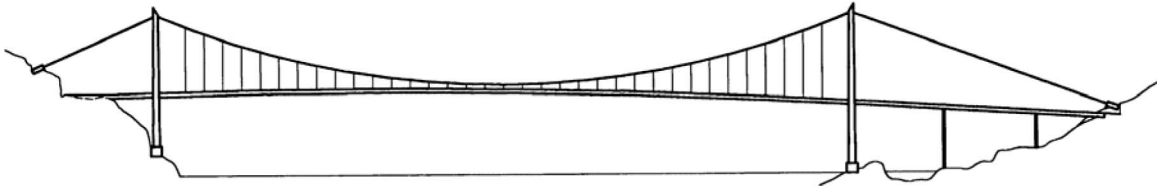


Figure 1. Elevation of Lysefjord Bridge with main span of 446 m.

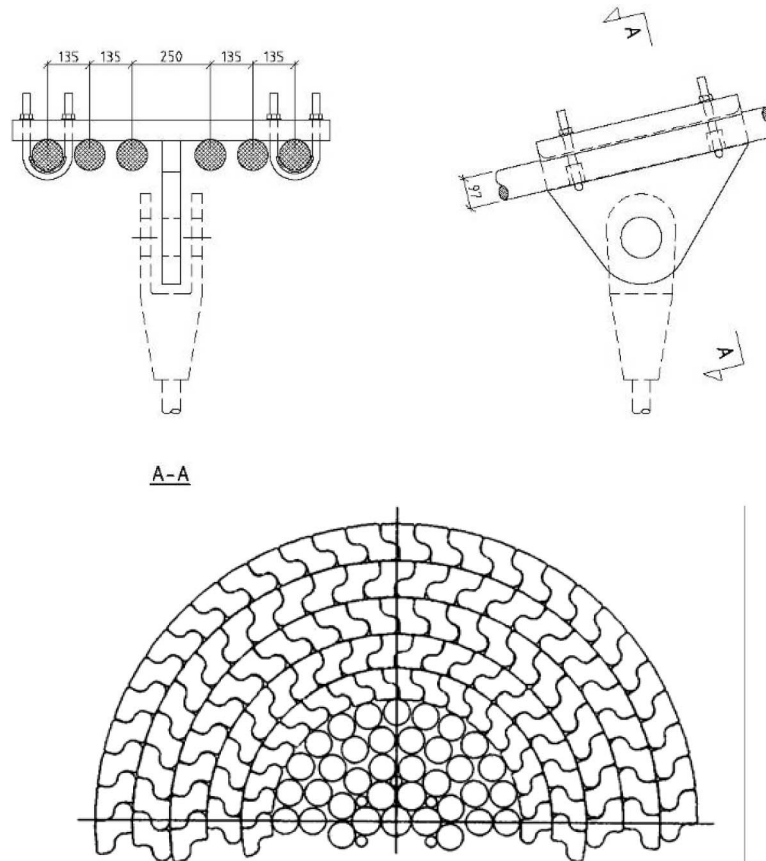


Figure 2. Cross-section of the main cable arrangement and suspender clamp in the main span, and details of the upper half of the cable cross-section.

performed at least twice a year. Figure 3 shows the total number of wire fractures based on visual observations.

The fractures are evenly distributed along the length of the cables, and there is no indication of accumulation of fractures at saddle points or suspender clamps. Around the circumference of the cable cross-section there is a tendency to slightly more registrations of fractures on the top side than elsewhere.

## 2. Failure analyses

Failure analyses were carried out for fractured 6 mm Z-wires from the outer layer of the main cables (Strengelsrud 1999, Leinum 2000, 2001). The wires are made of unalloyed carbon-steel according to EN-10016-4 with a

nominal tensile strength of 1570 MPa. The wires are hot galvanized with a 40- $\mu\text{m}$  thick zinc layer. The performed failure examination consisted of the following:

- visual examination;
- scanning electron microscope (SEM) and energy dispersive spectrometer (EDS) analyses;
- metallographic examination and hardness measurements; and
- comparison with wire fractures both at site and on photographs.

In addition, all wires in layer no. 10 (outer) to layer no. 8 (a total of 142 Z-wires with height 6.0 mm) of a 1.65-m cable section (left overs from cable production) were visually

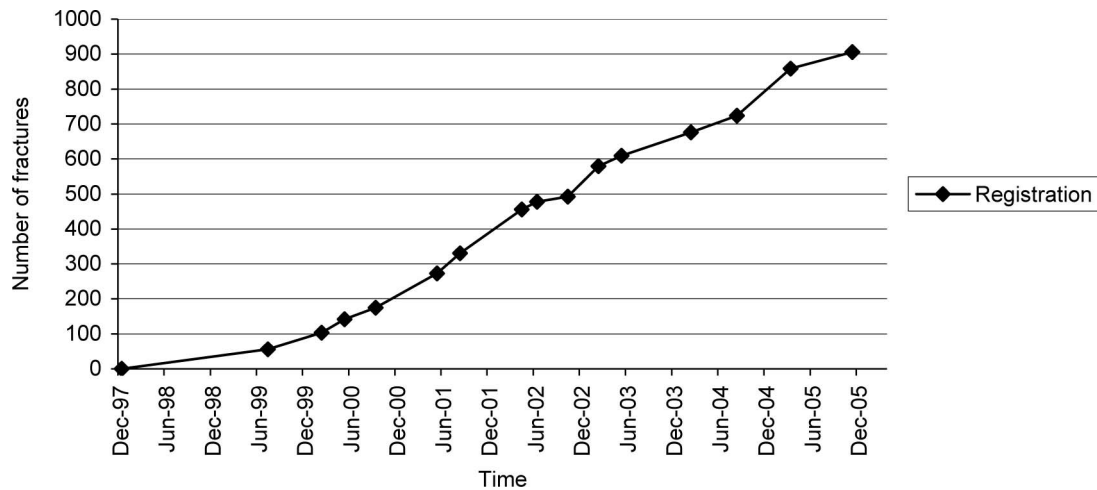


Figure 3. Time development of wire fractures (accumulated).

examined. The visual examination was performed both prior to and after dezincification of the individual wire surfaces.

### 2.1 Visual examination

The fractured wire samples were visually examined by use of a stereomicroscope at magnification 6–50 $\times$ . Most of the samples had been cleaned in inhibited hydrochloric (HCl) acid prior to reception, which means that the zinc layer and the presence of possible corrosion products were removed from the surfaces of the wires. However, figure 4 shows typical fractured Z-shaped wire sections where the paint and zinc layer are still present. The sketch in figure 5 illustrates the location of surface irregularities revealed after removal of the zinc layer.

All of the examined samples showed surface irregularities which were located at the same profile edge as the fracture initiation areas. An examination of an uncleaned fracture surface disclosed the presence of dark-coloured areas observed in the vicinity of the initiation area of the fracture. These areas were examined more closely using a SEM.

For the wire samples from the 1.65-m cable section, a restricted number of similar surface irregularities were disclosed during the examination of the individual Z-wires, but only after removal of the zinc layer.

### 2.2 SEM and EDS analyses

The fracture surface shown in figure 5 and the surface imperfections shown in figure 6 were examined more closely in a SEM connected to an EDS. The samples were cleaned in alcohol prior to the examinations being carried out.

Figure 7 shows characteristic SEM photos of the fracture surface and the surface imperfections. The SEM

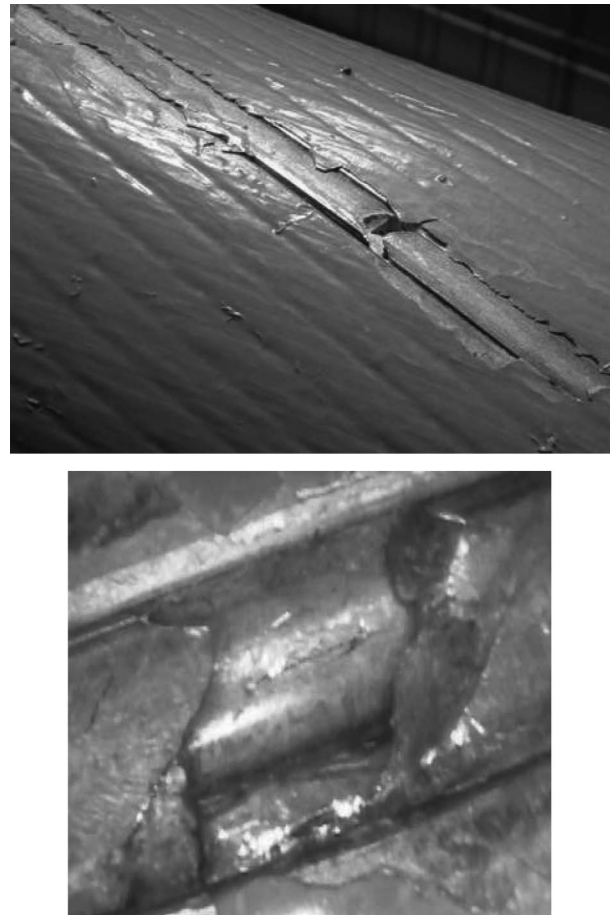


Figure 4. Photographs of fractured wire in cable at site.

examination revealed more defects than found during the visual examination. The general impression, with respect to the appearance of the imperfections, is that two types of

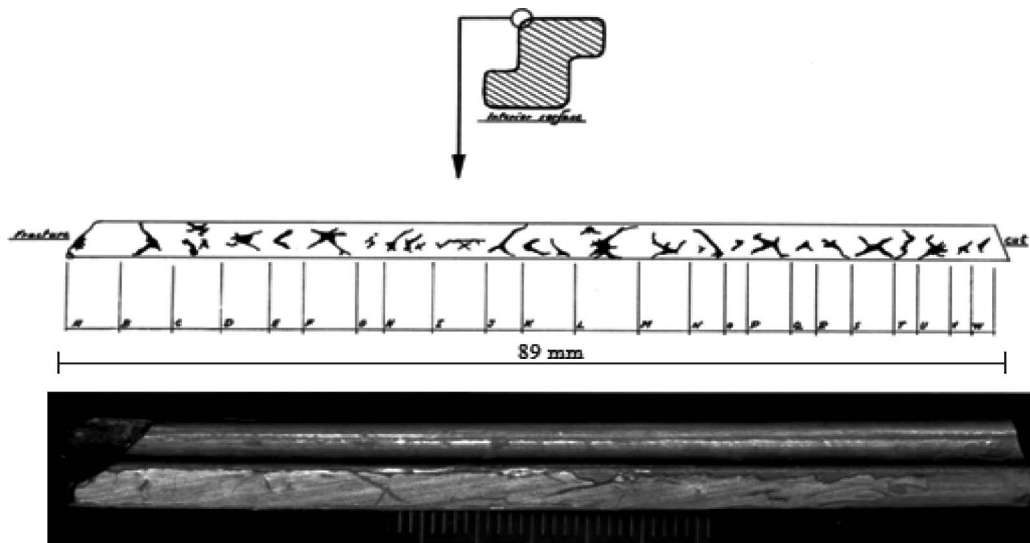


Figure 5. Overview of typical wire sample taken from the outer layer of one of the main cables. The arrow points to the fracture surface. The sketch illustrates numerous surface defects found along the exterior surface edge after removal of paint and zinc layer (from Strengelsrud *et al.* 1999, with permission).

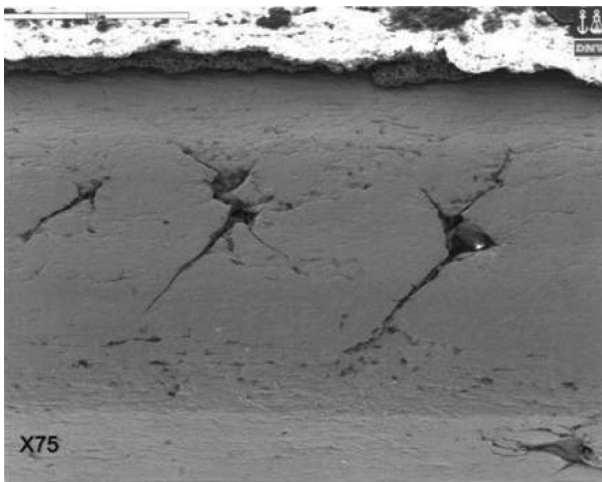


Figure 6. SEM photograph of some of the surface defects illustrated in figure 5. The zinc layer is removed.

imperfections were present: (1) cross-like geometry/shape resulting in lack of small pieces of surface material (see figure 6); and (2) surface imperfection most likely caused by some kind of surface material overlap during the geometrical forming (drawing/rolling) of the wire.

The majority of the imperfections were located at one profile ridge of the wire samples, the same ridge where the initiation areas were located. Figure 7b shows the general fracture mode being ductile with areas of brittle behaviour (cleavage) in between.

Qualitative element analyses, representing the general fracture surface of the wire and the initiation area were

carried out for one wire sample. The analysis diagram representative for the initiation area (see figure 8) strongly indicates the presence of zinc (Zn) at the fracture surface. Since no zinc was detected in the central part of the wire, this observation confirms that the surface imperfection was present in the steel wire when the wire was subjected to hot-dip galvanization.

### 2.3 Metallography

A specimen representing the longitudinal (axial) direction of the wire sample and sectioned through one of the defects was prepared for an optical metallography using standard procedures and further etched in a solution of 2% Nital.

Figure 9 shows the defect in etched condition. As expected, the microstructure is heavily deformed as a result of the manufacturing process. Distinct flow lines can be seen in the vicinity of the defect, indicating that the defect has been introduced during manufacturing of the Z-wire.

Microstructural examinations of several cross-sections of defects were performed for both fractured wires and the wires from the 1.65-m cable section. They all show an appearance similar to the one shown in figure 9. The most extensive defect examined was measured to have a depth of 0.175 mm from the wire surface. However, for some of the samples, narrow cracks, initiated and propagated from the bottom of the manufacturing defects, were observed. In this case, the most extensive defect examined (including the crack) was measured to have a depth of 0.65 mm measured from the wire surface.

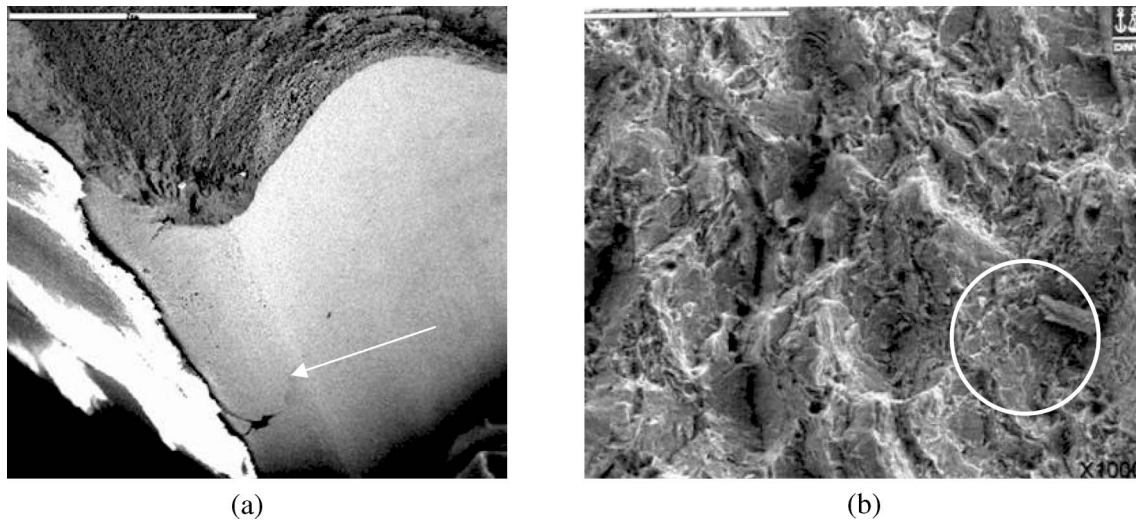


Figure 7. (a) The fracture surface pointed out in figure 5 and a surface defect in the adjacent area. SEM photograph, 25 $\times$ . (b) A ductile fracture mode with areas of brittle behaviour as marked out. SEM photograph, 1000 $\times$ .

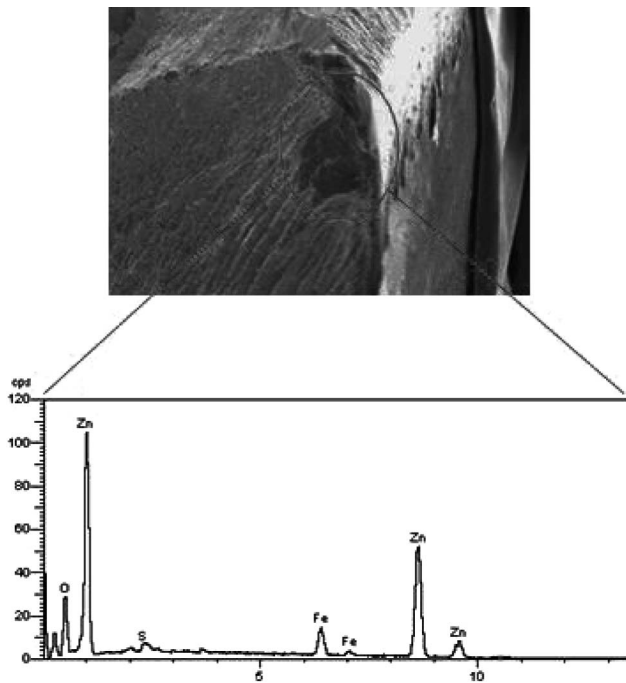


Figure 8. A qualitative element analysis diagram representative for the initiation area of the fracture (Leinum 2000).

#### 2.4 Hardness measurements

The hardness measurements were carried out using a Vickers hardness indenter and a 0.1 kp load (HV1). The measurements were carried out at the longitudinal cross-section of one selected wire.

The single values were recorded both from the wire surface and along the cracked area and from the

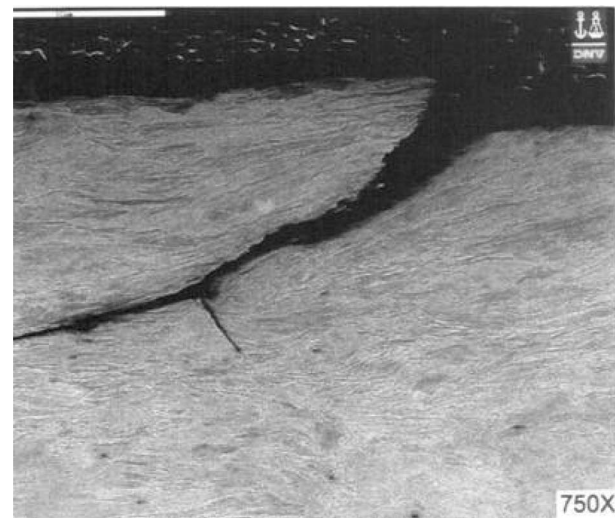


Figure 9. Cross-section of typical surface defect (750 $\times$ ) (from Strengelesrud 1999, with permission).

opposite wire surface. The results are graphically illustrated in figure 10, and show a hardness increase in the area close to the wire surface. This can probably be related to an increase in deformation in combination with a somewhat higher temperature caused by friction during the rolling process. The decrease in hardness just beneath the wire surface is connected to uncertainties in the performance of the measurements.

#### 2.5 Discussion of failure analyses

The different examinations of the failed 6-mm Z-wires revealed the presence of surface imperfections located

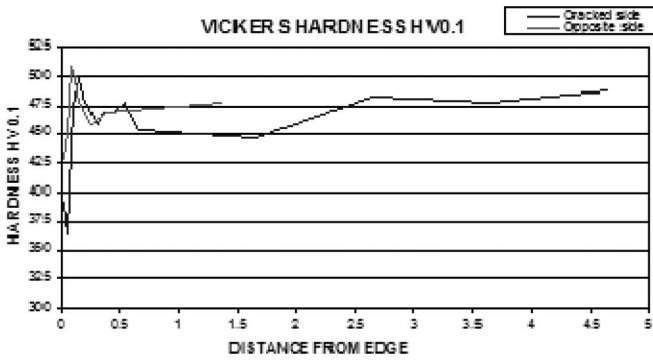


Figure 10. Hardness measurement (Leinum 2000).

mainly at one of the profile edges. The imperfections were observed at the steel surface of the wire, that is, after the zinc layer has been removed by immersing the wire in hydrochloric acid.

The wire fractures in question have most likely initiated in connection with imperfections that probably are similar to those observed along the edge profile of the wires. The statement is further verified with the aid of a cross-section through one of the observed imperfections, which clearly show that a crack has initiated and propagated from the bottom of the defect. Thus the Z-wires have probably suffered a tensile overload fracture after a reduction in the cross-section of the wire related to the presence of imperfections and further crack propagation from the defects.

The SEM and EDS analyses carried out on the fracture surface for one of the wire samples that had not previously been cleaned in acid showed that zinc was present at the fracture surface. The zinc was detected in the vicinity of the initiation area of the fracture and close to the surface of the wire. This confirms that the surface imperfections have been introduced prior to the galvanizing of the wires. Thus, it is likely that the observed imperfections have been created during the manufacturing, i.e. the rolling process. The surface appearance of the imperfections and the metallographic geometry also give the impression that the imperfections are a result of cold-flow overlap and/or local surface tearing during the plastic forming process of the wire.

The general fracture surface outside the initiation area consists of a ductile fracture mode in combination with brittle areas with a transgranular appearance in between.

No indications of external corrosion attacks or fatigue were found to contribute to the wire fractures. Additionally, no deleterious material constituent or abnormalities, other than the surface imperfections, could be observed in the examined cross-section of the wire sample. However, the presence of transgranular brittle areas located at the central part of the fracture surface of one of the wire samples might be a result of hydrogen embrittlement.

### 3. Criticality of surface irregularities on Z-wire

Because the wire fractures of the Lysefjord Bridge evidently initiated from surface irregularities, it was of interest to quantify the critical size of those irregularities. A fracture mechanics analysis, based on the British Standard BS7910, has been performed (BSI 2005).

The calculated critical size of surface irregularities is compared to the actual sizes observed on wires from the bridge. Finally, the result of the fracture mechanics analysis is compared to the non-destructive examination (NDE) of wire during production.

Three input parameters are important for a fracture mechanics analysis:

- (1) fracture toughness of the wire material;
- (2) tensile stress–strain curve of the wire material; and
- (3) loading condition of cable and wires.

#### 3.1 Fracture mechanics testing

Eight single edge notched bend (SENB) specimens were prepared from 6-mm Z-wire (type Z-60111) as illustrated in figure 11. The wires were spares from a previous investigation on the cables of the Lysefjord Bridge (Leinum 2001). The fatigue pre-cracking and fracture mechanics testing were performed according to the British Standard BS7448 (BSI 1991), at room temperature. The test set-up and an example of a fracture surface are shown in figure 12.

The results are presented in table 1. The characteristic fracture toughness of the wire is  $67.1 \text{ MPa m}^{1/2}$ . This is the second lowest results of the test series. The statistical recommendations used are given in BS7910.

The characteristic fracture toughness is just outside the validity range for  $K_{IC}$  ( $a_0, B \geq 2.5K_{IC}^2/\sigma_{YS}^2$ ). The small width ( $B$ ) and crack length ( $a_0$ ) of the test specimen limits the validity range. However, it is considered relevant to use the result in the fracture mechanics analysis if it is combined with an evaluation of what could be a slight overestimation of the fracture toughness.

#### 3.2 Tensile properties

As no stress–strain curve from the 6-mm Z-wire was present, a typical curve for similar material was adopted. The strength level and ductility of the adopted curve was adjusted to fit the reported yield strengths, tensile strengths and ultimate elongations of the production tests of the cables of the Lysefjord Bridge. The results are presented in table 2 and the stress–strain curve is presented in figure 13.

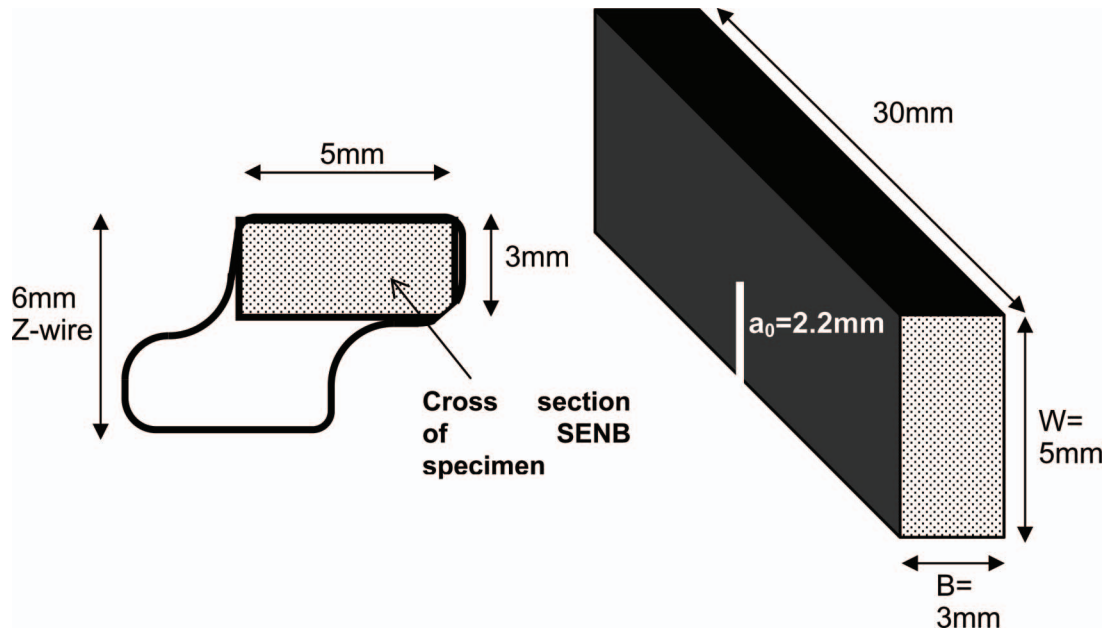


Figure 11. Preparation of SENB specimen from Z-wire.

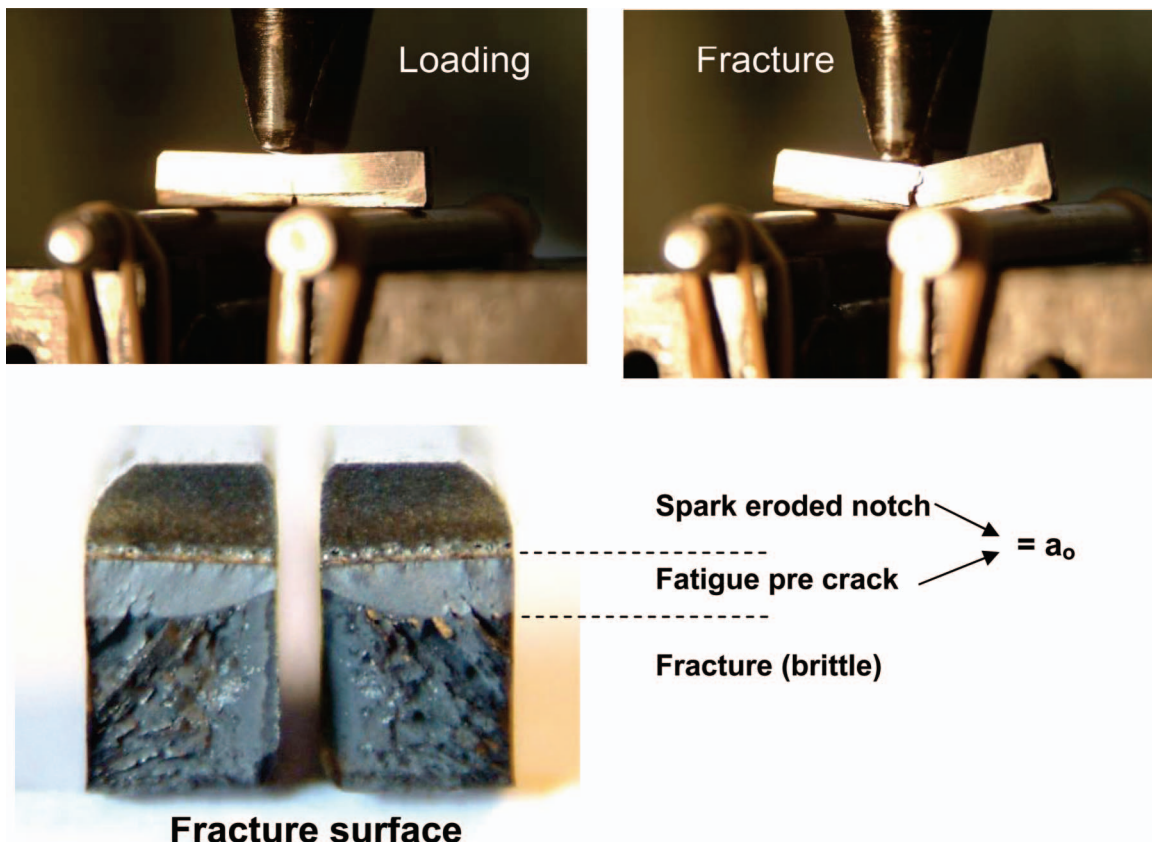


Figure 12. The test setup and a typical fracture surface after testing.

Table 1. Dimensions of SENB specimens and results from the fracture mechanics testing.

Test specimen no.	Dimensions			Max. load (kN)	Toughness, $K$ (MPa m <sup>1/2</sup> )	Type of fracture
	$B$ (mm)	$W$ (mm)	$a_0$ (mm)			
A29-1	2.98	4.96	2.24	1.62	71.7	brittle
A29-2	2.97	4.97	2.09	1.69	68.2	brittle
A29-3	2.96	4.98	2.24	1.52	67.1	brittle
A29-4	2.97	4.97	2.24	1.43	62.9	brittle
A38-1	2.93	4.96	2.05	1.69	67.6	brittle
A38-2	2.99	4.98	2.00	1.78	67.6	brittle
A38-3	3.00	4.97	2.01	1.80	69.0	brittle
A38-4	2.99	4.96	2.06	1.74	68.8	brittle

Table 2. Tensile properties of 6-mm Z-wire used in the analysis.

E-modulus (GPa)	Yield strength, $\sigma_{YS}$ (MPa)	Tensile strength, $\sigma_{TS}$ (MPa)	Strain at max. load, $A_{gt}$ (%)
215	1490	1650	4

### 3.3 Loading conditions on wires

The design loading of the cables, inclusive of the maximum traffic loading, corresponds to a maximum nominal stress of 588 MPa along the cable length, i.e. 40% of the minimum required tensile strength of the cable.

The spinning process during cable construction applies a significant residual stress level in the wires. Therefore a residual stress level equal to the yield strength is assumed in the fracture mechanics analysis.

### 3.4 Fracture mechanics analysis

The software tool Crackwise ver. 3.15 was used for the calculations. The software is based on BS7910, and a level 2B assessment was performed. A geometrical simplification of the Z-wire was required (see figure 14). The critical size for surface irregularities for the given loading condition is presented in figure 15.

### 3.5 Discussion of the fracture mechanics analysis

The analysis on 6-mm Z-wire indicates that a surface irregularity with depth around 0.2 mm is critical regarding fracture. However, the deeply notched SENB specimen has higher constraint of the crack compared to a more shallow surface irregularity. A consequence of such geometrical effect is that the fracture toughness of surface irregularities is higher than the fracture toughness used in the present analysis, hence the critical defect size is actually larger. However, the contrary was observed due to the environmental effect on the bridge. The development of wire fractures has a shown similar trend for many years, and a

long-term environmental effect is evident. The environmental effect is most likely caused by hydrogen embrittlement, which could significantly reduce the fracture toughness. The environmental effect could most probably reduce the fracture toughness much more than the constraint of a shallow surface irregularity could increase it. This means that the critical defect sizes of figure 15 most probably are non-conservative, i.e. the actual critical defect sizes are smaller.

It is likely that the stress distribution between wires is not homogeneous. For wires with higher applied stress, i.e. >40% of the minimum required tensile strength of the cable, the critical size of surface irregularities is reduced compared to figure 15.

It should be noted that the NDE of wires during production is performed with the eddy current method. The resolution is 0.2 mm depth, but larger irregularities have been found during examination of wires (Leinum 2001). The NDE procedure does not state the probability of detection (POD). However, the lower limit for detection of surface irregularities during production is at or above what is considered to be the critical depth of those irregularities. The relevance of the NDE is therefore questioned, and the need for better NDE methods/procedures to increase the resolution and POD is evident.

## 4. Corrosion protection system

Individual steel wires are protected against corrosion by hot-dip galvanizing. Through the galvanizing process a zinc layer (*later called zinc coating*) with thickness 40  $\mu\text{m}$  is developed on the carbon steel wires. This zinc coating that has good adhesion to the carbon steel substrate through metallurgical bonding, is less noble than carbon steel and will protect carbon steel against corrosion. However, the zinc layer will corrode when exposed to humid environment. The corrosion rate depends on the corrosivity of the actual atmosphere. For a structure exposed to marine environments, such as the Lysefjord Suspension Bridge, a uniform corrosion rate in the range 0.5–8  $\mu\text{m}/\text{year}$  is normally seen on the zinc coating (Leygraf and Graedel 2000).

After the galvanizing process it is important to store the galvanized wires in a way that ensures that the zinc coating

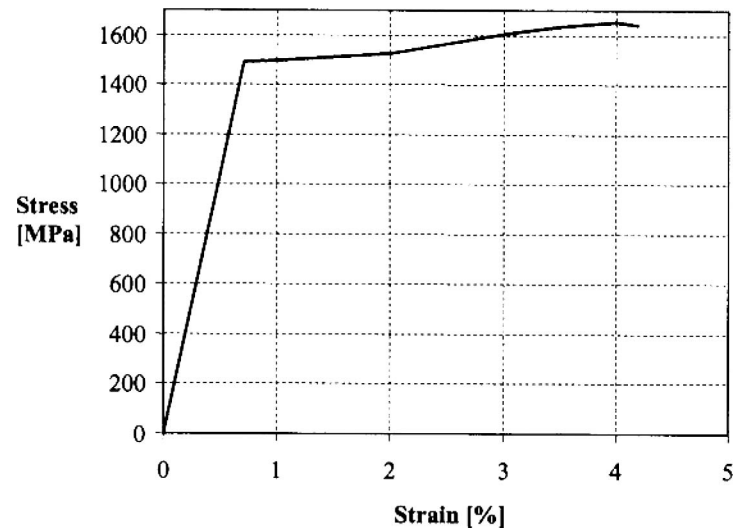


Figure 13. Adopted stress–strain curve to fit results from the production tests of 6-mm Z-wire.

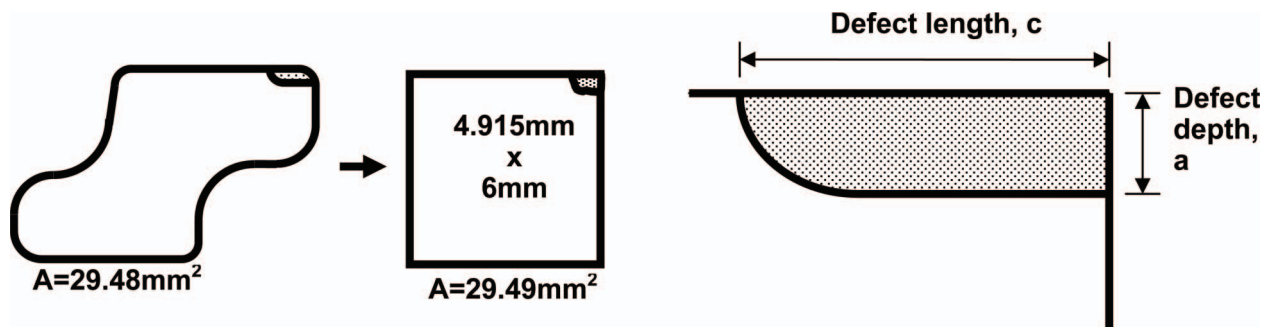


Figure 14. Illustration of the geometrical simplification of the Z-wire and the position and geometry of the typical corner defect.

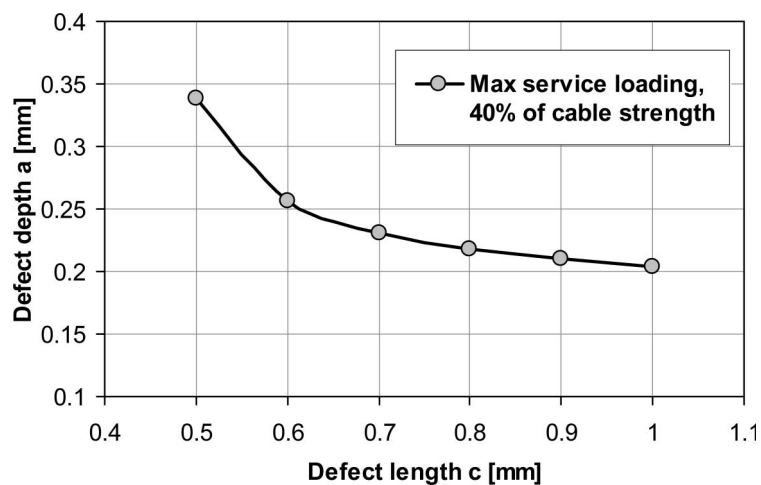


Figure 15. Critical defect sizes for 6-mm Z-wire at the given loading condition.

corrodes to form a dense, adherent, and protective basic zinc carbonate [ $3\text{Zn}(\text{OH})_2 \cdot \text{ZnCO}_3 \cdot \text{H}_2\text{O}$ ] that resists further corrosion. If the basic zinc carbonate is not formed, a porous,

less tenacious and non-protective zinc carbonate [ $\text{ZnCO}_3$ ] is formed instead. In humid environments, corrosion will rapidly occur, causing the *white rust* phenomenon. *White*

*rust* has the appearance of a thick, white and waxy deposit. Once white rust forms, it is difficult and expensive to prepare the surface for painting. Even minor residues of white rust under paint lead to paint failure. It is of vital importance to prevent the development of white rust by ensuring sufficient access to air during storage and transportation of wires.

To extend the lifetime of a galvanized steel component, a layer of organic coating can be put on top of the zinc coating. The organic coating layer will prevent direct contact with the surrounding atmosphere (or water) and thereby reduce the corrosion rate of the zinc coating. Application of an organic coating layer on the individual wires is not a practical solution. However, for the final cable a three-layer epoxy coating from Carboline was applied. Figure 16 illustrates the final corrosion protection system that was used for the cables.

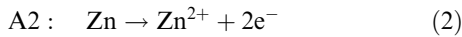
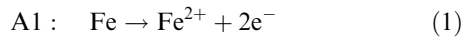
The cable used on the Lysefjord Suspension Bridge was produced on site with galvanized steel wires transported on drums from the fabrication site. During the cable spinning, it was observed that the spinning compound was brittle and that it was partly squeezed out. The spinning compound was used to reduce the friction between the individual wires during construction.

During the first 6 months after installation the cables were exposed *without* the organic coating as described above. During this exposure period the zinc coating was the only corrosion protection system for the cables.

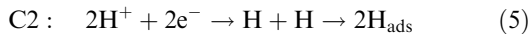
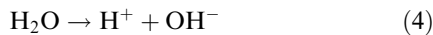
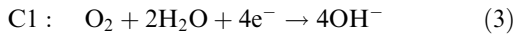
## 5. Corrosion reactions

Carbon steel and zinc will corrode when exposed to a humid environment. However, due to the development of a protective zinc carbonate layer the corrosion rate of zinc (*self corrosion*) is relatively low. When electrically connected and submerged in the same electrolyte, a galvanic cell will be established between the two alloys. In this cell, zinc is the less noble alloy and will protect carbon steel against corrosion. Figure 17 shows a schematic of the overvoltage curves for anodic and cathodic reactions:

anodic reactions:



cathodic reactions:



In neutral water, zinc will corrode at the corrosion potential of zinc ( $EC_{\text{Zn}}$ ) close to  $-1000$  mV Ag/AgCl defined by the anodic reaction according to equation (2) and cathodic reactions according to equations (3)–(5). Carbon steel will corrode at the corrosion potential of ( $EC_{\text{Fe}}$ ) which is close to  $-600$  mV Ag/AgCl defined by the anodic reaction according to equation (1) and cathodic reactions according to equation (3)–(5). When electrically connected, zinc will protect carbon steel from corrosion with a coupling potential (called galvanic corrosion potential EG) in between  $EC_{\text{Fe}}$  and  $EC_{\text{Zn}}$ .

Figure 17 also shows the cathodic curves for equations (3)–(5). As can be seen from the curves, the development of hydrogen increases with more negative potentials. This means that corrosion of zinc will promote the development of hydrogen atoms.

The positions of the overvoltage curves and the development of hydrogen depend on environmental parameters such as, for example, temperature, availability of oxygen and composition and pH of the water film (humidity).

## 6. Hydrogen-induced stress cracking

Carbon steel and other alloys can suffer from *hydrogen-induced stress cracking* (HISC) under certain conditions. The following elements need to be present to initiate hydrogen-induced stress cracking:

- (1) certain hydrogen content;
- (2) certain local stress–strain level; and
- (3) alloy with microstructure susceptible to hydrogen-induced stress cracking.

The susceptibility is also increased with: (1) presence of local surface cracks and (2) high strength materials.

The hydrogen content in a metal can be a result of surface cleaning and/or surface treatment. In addition, welding and corrosion can generate hydrogen. Absorbed hydrogen ( $H_{\text{abs}}$ ) will be transported in the metal by diffusion. The flow of hydrogen (permeation)  $J_{\text{H}}$  follows Fick's law:

$$J_{\text{H}} = -D_{\text{H}} \frac{\partial C_{\text{H}}}{\partial x} \quad (8)$$

where  $D_{\text{H}}$  is the diffusion coefficient and  $C_{\text{H}}$  the concentration of hydrogen in the metal for one-dimensional flow. See figure 18 for a schematic view of equations (5)–(7) and diffusion assuming corrosion on the zinc coating covered by a water film.

However, in practice hydrogen transport in a metal is more complex due to the fact that hydrogen can be trapped in the metal (reversible and/or irreversible traps). In addition the hydrogen transport is influenced by the stress–strain level in the vicinity of a crack (Olden *et al.* in press).

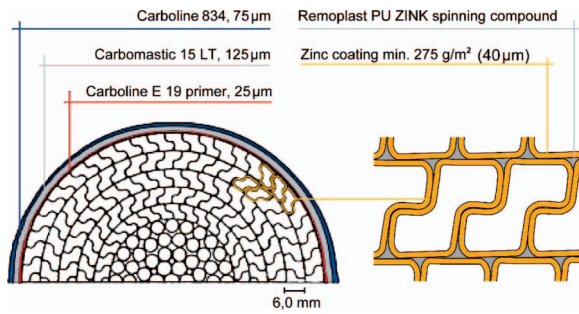


Figure 16. Corrosion protection for individual steel wires and the complete cable.

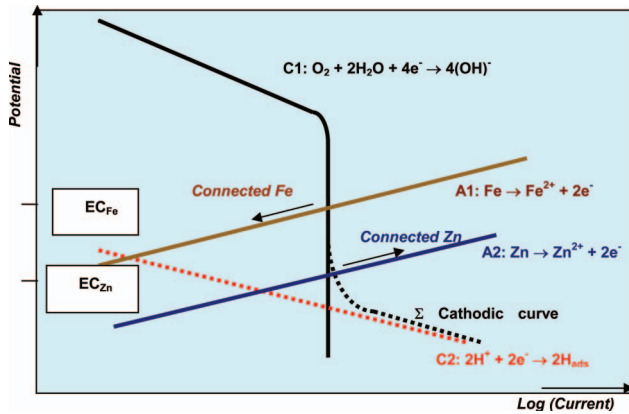


Figure 17. Schematic overvoltage curves for carbon steel (Fe) and zinc (Zn) showing connected and not-connected conditions.

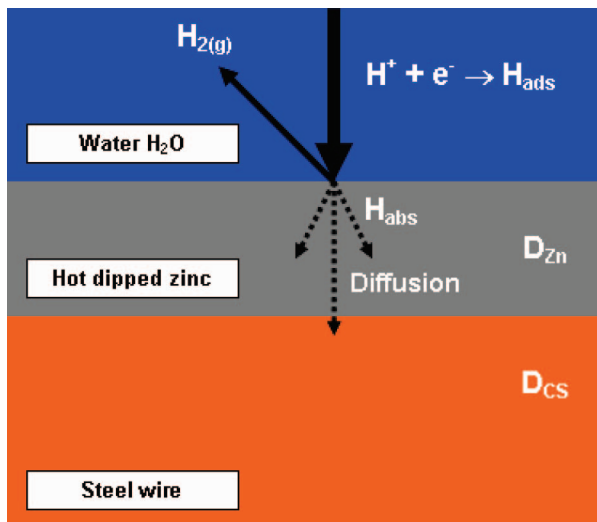


Figure 18. Schematic of hydrogen generation through the corrosion reaction of zinc and diffusion through the zinc coating into the steel wire ( $D_{Zn}$  and  $D_{CS}$  are diffusion coefficients for zinc and carbon steel, respectively).

## 7. Possible reasons for the wire fractures

### 7.1 Wire fracture caused by corrosion of bare steel wires

As long as the wires are covered by the zinc layer, corrosion of the carbon steel substrate material will be prevented by the less noble zinc. If greater areas of the zinc coating is 'missing' leading to exposure of the substrate carbon steel material – by poor process control during galvanizing or by mechanical damage during fabrication – corrosion will occur on carbon steel. If corrosion of carbon steel occurs for a long period, the load-carrying area of the actual wire will be reduced and at a certain point the wire will break due to overload. This type of corrosion has been reported in the literature (Cao *et al.* 2002). However, pictures of broken wires shows that this reason can be excluded for the wire failures on the Lysefjord Suspension Bridge – see figure 4 showing examples of two broken wires.

### 7.2 Wire fracture caused by hydrogen-induced stress cracking

**7.2.1 Hydrogen from the hot-dip zinc process.** During the hot-dip galvanizing process the steel wire is rinsed through a pickling process using an electrolyte containing  $H_2SO_4$  or  $HCl$ . During this process hydrogen will be released and can act as a source for hydrogen absorption in the steel wires. The development of hydrogen can be eliminated by introducing an inhibitor into the electrolyte or the absorbed hydrogen can be removed (baked out) through heat treatment at  $240^\circ C$  for 4 h after galvanizing. Experience has shown that hydrogen can be entrapped in the substrate material covered by a zinc layer for a very long time. The diffusion coefficient for hydrogen in carbon steel,  $D_{CS}$ , is in the range  $10^{-7} \text{ cm}^2/\text{s}$  compared to  $D_{Zn}$  equal to  $10^{-11} \text{ cm}^2/\text{s}$  for the zinc layer (Cao *et al.* 2002).

**7.2.2 Hydrogen from corrosion of zinc on a surface without organic coating.** Zinc exposed to a marine atmosphere will corrode with a corrosion rate less than  $10 \mu\text{m}/\text{year}$  (Olden *et al.* in press). Due to the corrosion potential of zinc in the range  $\approx -1000 \text{ mV Ag/AgCl}$ , the cathodic reaction will be a combination of equations (3) and (4). The adsorbed hydrogen  $H_{ads}$  can then either be absorbed in the zinc coating as diffusible hydrogen or recombine and produce hydrogen gas  $H_{2(g)}$  according to equation (7). The amount of absorbed hydrogen depends mainly on the temperature, availability of oxygen, pH of the water and the surface condition. Figure 19 shows schematically how absorbed hydrogen diffuses through a local crack in the steel wire.

This will be the situation during the initial period without the organic coating on the cable and after organic coating is applied in areas without coating due to mechanical damage or degradation.

Experience from other installations with galvanized steel without organic coating exposed to similar environmental conditions indicate that this situation will not generate enough absorbed hydrogen (combined with local stress–strain level) to initiate hydrogen-induced stress cracking. This is also confirmed in Betti *et al.* (2005) where no increase in hydrogen content could be measured on a galvanized wire after exposure to corrosive environment. However, for long-term exposure (years) this can be a source for increased hydrogen in high strength steel wire.

**7.2.3 Development of hydrogen in local areas without zinc and organic coating.** Local areas can be without zinc coating due to poor process control during the hot-dip galvanizing process, mechanical damage during fabrication or corrosion of the zinc layer. The less noble zinc layer will cathodically protect the carbon steel and the effectiveness of the cathodic protection depends on the thickness of the water film on the surface. Through this process zinc will corrode (and carbon steel protected), while the corresponding cathodic reactions will be according to equations (3)–(7). This could lead to the absorption of hydrogen on the bare steel surface.

This situation is only valid as long as the steel wires (or the final cable) are without an organic surface coating.

**7.2.4 Local water volumes beneath organic coating on the cable causing corrosion.** To extend the lifetime of the cables, a three-layer organic coating was applied on the final cables after 6 months. The organic coating layer will prevent direct contact with the surrounding atmosphere (or

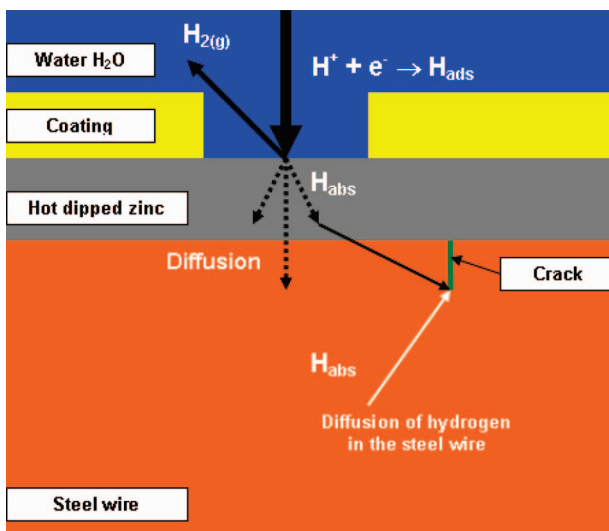


Figure 19. Schematic of a steel wire with damaged organic coating covered with a water film where zinc corrosion generates hydrogen that is partly absorbed and diffused into the metal.

water) and thereby reduce the corrosion rate of the zinc layer. However, both water and oxygen will diffuse into/through the organic coating. As long as the coating is bonded to the zinc layer, no accumulation of water will occur and corrosion of the zinc layer is prevented. However, if the bonding is lost water will accumulate in the volume between the organic and the zinc coating and corrosion of zinc will occur. The corrosion rate depends on the chemistry of the water and the diffusion rate of oxygen. In the literature, permeability values have been reported in the range 10–30 g/m<sup>2</sup> per day for water through a 300- $\mu$ m thick epoxy coating (Funcke *et al.* 1978). Figure 20 shows a schematic of this situation with corresponding anodic and cathodic reactions, assuming both reactions occurring in the water volume beneath the intact organic film.

Figure 21 shows a schematic of a volume where the spinning compound is lacking and the volume is filled with

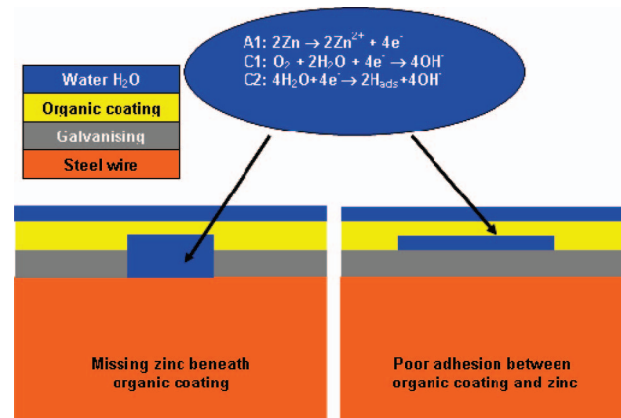


Figure 20. Schematic presentations of local water volumes beneath an organic film with poor adhesion to the zinc coating.

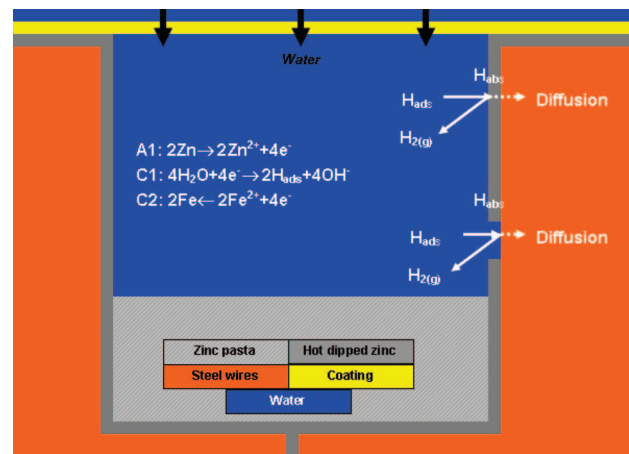


Figure 21. Schematic of a volume, where parts of the volume to be filled with 'spinning compound' is filled with water diffused through the organic coating. In this case, damage in the zinc-coated area is included.

water that is diffused through the organic coating. As long as water penetrates the organic coating corrosion will occur on the zinc coating according to equation (2) with corresponding cathodic reactions according to equations (3)–(6). As can be seen from equations (3)–(4), water will be consumed as a result of the corrosion reaction. The corrosion rate will probably depend on the diffusion rate of water through the organic coating film.

If the cable contains small volumes without spinning compound that is not filled up with the organic coating, the process described above can occur. Since the cable is normally surrounded with a humid layer part of the year, the described process is probably an on–off process during the year. It will probably also vary along the cable and along the circumference of the cable. *However, it is an effect that can explain the continuous development of new fractures in the steel wires.*

### 7.3 Can the fracture development as a function of time be explained with hydrogen?

The possible corrosion ‘types’ described in 7.2.2–7.2.4 above will generate hydrogen atoms available for absorption into the zinc coating and the steel wire. Since these reactions will occur over time (as long as water is available on the metal surface), a possible source for supply of hydrogen to the fracturing process is available.

## 8. Evaluation of load-carrying capacity

Full-locked coil cables have an important advantage in connection with wire fractures. The reduction in load-carrying capacity caused by one single fracture is limited to the position where the fracture occurs. Because of the locking between the wires caused by the Z-shape and the spiral spinning, the load capacity is recovered in a distance less than 2 m from the fracture. This hypothesis is based on visual observations of cracks in the paint coating along the fractured Z-wire. The wire has recovered its loading where the paint crack ends. Consequently, if there is sufficient distance between successive fractures, a great number of fractures may cause no more strength reduction than one single fracture.

This is of course a great advantage, but makes it very difficult to calculate the strength reduction of a cable with a given number of fractures. To be able to assess the consequence, it is necessary to know the exact position of each fracture and the distance where the force is recovered in the wire.

However, a common and conservative method is simply to sum the effect of every fracture within a length of 3 m, which is a common length of the crack in the paint coating along a fractured Z-wire. Since the cable is not stronger than its weakest part, the 3 m with the highest number

of fractures will represent the remaining load-carrying capacity.

One single fracture in the outer layer of one of the cables of the Lysefjord Bridge represents about 0.4% loss of strength. If the highest frequency within a distance of 3 m (some place on the cable) is  $n$  fractures, the total loss of strength is  $n \times 0.4\%$ . However, the situation may be worse because the condition of the sub-layers is unknown. Wire fractures in the sub-layers must be added if, but only if, they are situated within the same 3 m.

The most damaged cable, i.e. no. 4, contains a total of 187 fractures in the outer layer, which gives an average mutual distance of 3.7 m. Unfortunately, the first inspections did not record the exact position of the fractures. This, in addition to the fact that the condition of the sub-layers is unknown, makes it impossible to calculate the exact remaining capacity of the cables.

However, most of the fractures are recorded quite accurately so the approximate remaining strength of each cable can be calculated. Omitting the effect of fractures in the inner layers and using the 3-m rule, cable no. 4 comes up with a strength reduction of about 1.1%, and the whole cable group results in an average strength reduction of 0.6%.

If it is difficult to calculate the exact reduction of load-carrying capacity due to recorded fractures, it is even more intricate to evaluate the future reduction. Different methods of probability calculations could possibly give reliable answers, but the lack of knowledge of the exact positions of existing fractures reduces the value of such analyses.

The expectation was that the growth of fractures would decrease and even stop after some years. However, the growth has been almost constant since installation and is still between 120 and 150 wire fractures per year.

This fact is quite alarming and makes the need for strengthening or even full replacement of the cables, in not too many years, quite probable. Even more worrying is the fact that although the registrations show a linear growth of fractures, the decrease in capacity will hardly be equal, but worse. As mentioned, the crucial factor is not the total number of fractures, but the concentration within an arbitrary 3 m length of the cable. Because of the random distribution of the fractures, some places will get higher concentrations than others and therefore the local diminution will be worse than what the total growth of fractures would render.

Hence, frequent inspections of the cables are very important. Up to now, a thorough visual inspection has been carried out every 6 months. In addition, an acoustic monitoring system will be installed, a system with several sensors listening for the typical sound of a wire fracture. Due to the time differences between the different sensor recordings, the system will be able to determine the position

of every new fracture. Consequently, this system makes it possible to record future fractures also in the sub-layers.

### 9. Long-term experience with locked coil cables in Norway

Many Norwegian suspension bridges built 50–80 years ago are small bridges with main span length 80–200 m. During the last 50 years NPRA has built 24 suspension bridges with main span length between 200 and 850 m. NPRA has generally good experience with locked coil cables and reported problems are due to reasons other than the quality of the cables, i.e. wire fractures due to oscillations caused by wind, and wire fractures due to heavy corrosion related to poor maintenance.

Single-span suspension bridges have a rather long free cable length between tower top and anchorage. If the damping arrangement to mitigate oscillations is insufficient, wire fractures may occur at the edge of the saddle and close to the socket. Several bridges with these kinds of problems are registered. When sufficient damping arrangement is installed, the problem is eliminated.

Wire fractures related to a bad design of details close to the anchorage is reported. Poor design may cause heavy corrosion and extensive wire fractures, and strengthening of the cable necessitated by corrosion has been performed. Galvanizing of cable wires and zinc spraying of steel details has been common practice since the 1960s. Paint is the only corrosion protection for bridges older than about 40 years. On all bridges older than about 40 years corrosion has been observed under suspender clamps. Heavy corrosion was observed on the Varodd Bridge built in 1956. The bridge suffered from poor detailing of suspender clamps with sharp edges, and close to these more than 100 wire fractures were observed. However, maintenance work 25 years ago eliminated that problem.

The kind of wire fracture problem reported for Lysefjord Bridge is unique. Comparable fracture problems have not been registered on any of the 60 suspension bridges that are operated by NPRA, and many of them are 50 years old.

No wire fractures (or only a few) are the common observation on most Norwegian suspension bridges built 30–60 years ago. Obviously, sufficient knowledge exists to produce cables of good quality. Could the problem be that the requirement for cost-effective production has increased so much that it leads to reduction of quality regarding production of cable wires and cables?

### 10. Conclusion

Based on the failure examinations performed, the following conclusions have been drawn:

- The manufacturing, i.e. the rolling process, has created surface imperfections observed at the Z-wire edges.

- Cracks have initiated and propagated from the bottom of the surface imperfections.
- The Z-wires have most likely suffered a tensile overload fracture after a reduction in the cross-section of the wire, related to the presence of imperfections and further crack propagation from these defects.
- No indications suggesting that either corrosion or fatigue has contributed to the fracture were found.
- No deleterious material constituent or abnormalities, other than the surface imperfections, was observed.
- Hydrogen embrittlement may have contributed to the failure as a result of the cleaning process that the wires are exposed to prior to galvanizing.

Fracture mechanics testing of 6 mm Z-wire has been performed. The behaviour was brittle and a characteristic fracture toughness ( $K_{Ic}$ ) of 67 MPa m<sup>1/2</sup> was determined.

The fracture mechanics analysis showed that surface irregularities with depths around 0.2 mm could be critical regarding fracture of 6-mm Z-wire. If hydrogen embrittlement and inhomogeneous stress distribution between wires are included, the critical depth is smaller than 0.2 mm.

Hydrogen-induced stress cracking is the most probable reason for the time-dependent fracturing of the Z-wires. Possible sources for hydrogen are: (1) absorption during the pickling process as part of the hot-dip galvanizing process and (2) corrosion of the zinc coating after installation of the suspension cables due to:

- damaged organic coating;
- damaged organic coating and zinc coating locally; and
- diffusion of water and oxygen into local areas with poor adhesion between the organic coating and the zinc coating.

The wire fracture problem reported for Lysefjord Suspension Bridge is unique in Norway.

### References

- Betti, R., West, A.C., Vermaas, G. and Cao, Y., Corrosion and embrittlement of high strength wires of suspension bridge cables. *J. Bridge Engng.*, 2005, **10**(2), 151–162.
- BSI., *British Standard BS7448-1: Method for Determination of K<sub>IC</sub>, Critical CTOD and Critical J Values of Metallic Materials*, 1991 (BSI, London).
- BSI., *British Standard BS7910: Guide on Methods for Assessing Acceptability of Flaws in Metallic Structures*, 2005 (BSI, London).
- Cao, J.L., Li, L.T., Wu, J.X., Lu, Y.P. and Gui, Z.L., Diffusion of hydrogen in a steel substrate absorbed during zinc and zinc-silica electroplating. *Corrosion*, August 2002, **58**, 698–702.
- Funcke, W., Machunsky, E., Handlooser, G., *Farbe und Lack*, 1978, **84**, 152–159.
- Leinum, B.H., *DNV Report No. 200-1250. RV13, Lysefjord Bridge; Examination of Failed Z-wire Rods*, 2000 (DNV-Oslo).

Leinum, B.H., *DNV Report No. 2000-1250; RV13, Lysefjord Bridge; Examination of a 1.65 m Main Cable Section*, 2001 (DNV-Oslo).  
Leygraf, C. and Graedel, T., *Atmospheric Corrosion*, 2000 (John Wiley & Sons, Chichester).  
Olden, V., Thaulow, C. and Johnsen, R., Hydrogen diffusion and cracking in supermartensitic, duplex and super duplex stainless steel—a state of the art review. *Theoret. Appl. Fract. Mech.*, in press.

Strengelsrud, K., *DNV Report No. 1999-1348; Examination of a Fractured Section of Wire from a Main Cable of the Lysefjord Bridge*, 1999 (DNV-Oslo).